LASER SPECTROSCOPY OF COLOR CENTERS IN YTTRIUM ALUMINUM GARNET

BY

JOHN DARBY HEWITT

THESIS

Submitted in partial fulfillment of the requirements
for the degree of Master of Science in Electrical and Computer Engineering
in the Graduate College of the
University of Illinois at Urbana-Champaign, 2010

Urbana, Illinois

Adviser:

Professor J. Gary Eden

ABSTRACT

Nd:YAG lasers have become ubiquitous as tools for spectroscopy, materials processing, and medical care. It is well known by crystal growers that lattice defects in Nd:YAG can stifle laser efficiency, but to date very little has been done to isolate and characterize individual YAG defects. Knowing the spectral characteristics of these defects would make detection of distinct defects in a sample possible. This thesis describes a set of experiments performed to characterize these defects spectroscopically.

ACKNOWLEDGMENTS

I would like to thank my adviser, Professor J. Gary Eden, for his direction, encouragement, and enthusiasm. Thanks also to Tom Spinka for working closely with me on this project and to all my colleagues at the Laboratory for Optical Physics and Engineering for their experimental assistance. I am grateful to Carl Johnson and the II-VI Foundation for funding this project. Thanks also to Andrey Senin and VLOC for providing the samples used in this research. A special thank you goes to my wife and family for their undying support.

TABLE OF CONTENTS

CHAPTER 1

MOTIVATION AND HISTORICAL BACKGROUND

Since their discovery in 1964, neodymium-doped yttrium aluminum garnet (Nd:YAG) lasers have become ubiquitous as tools for spectroscopy, materials processing, and medical care [1]. Lattice defects in Nd:YAG are known to stifle laser efficiency by absorbing pump and lasing photons, but to date very little has been done to characterize YAG defects [2, 3]. As a result, laser crystal manufacturers have limited understanding of the influence of crystal growth parameters on the presence of potentially detrimental defects in Nd:YAG. The goal of this thesis is to investigate the energy structure and flow of energy between these defects using spectroscopic techniques. Knowing this energy structure and understanding the energy dynamics within the medium will make defect isolation and characterization possible, eventually leading to better optimized growth recipes for Nd:YAG laser crystals.

Color centers in YAG ($Y_3Al_5O_{12}$) are point defects in the lattice which have optical absorption bands that are within the ideally transparent wavelength range for YAG ($\lambda \geq 185$ nm) [4]. For defects to have absorption features within the transparency range of YAG, these defects must have energy states that reside between the valence band and the conduction band [5]. Most defects involve a deviation from the exact stoichiometry of the medium. For instance, standard doping of YAG with one or more rare-earth ions is considered a defect (known as an N-center) because it modifies the crystal stoichiometry, replacing a small percentage of the Y^{3+} ions with trivalent rare-earth ions such as Nd^{3+} [6]. The spectral features attributed to these "defects" make laser action possible in YAG.

The most commonly reported defect in YAG is an oxygen vacancy in the lattice with one or more trapped electrons, which is known as an F-center. The potential well at that position is sufficiently deep to trap one or more electrons freed from nearby ions [7]. Another physical defect often mentioned in the literature is the O^--center, which is created when high-energy

photons free an electron from an O^{2-} ion. This process has been shown to be enhanced by the presence of large ions—such as trivalent or tetravalent rare-earths—near the O^{2-} ions [8]. The freed electrons could be trapped by the nearby tetravalent or trivalent rare-earth ions, but they could also be trapped by nearby oxygen vacancies, thereby forming F-centers [8,9]. Table 1.1 summarizes the physical nature of these and several other YAG defects reported in the literature.

Table 1.1: Summary of YAG defects reported to date

Name	**Physical Description**	**Reference**
N-center	Normal doping configuration (RE^{3+} replaces Y^{3+})	[6]
A-center	RE^{3+} replaces Al^{3+}	[6]
P-center	N- and A- centers in close physical proximity	[6]
F-center	Oxygen vacancy with trapped electron(s) $\mathbf{F}^+$ 1 trapped electron $\mathbf{F}$ 2 trapped electrons $\mathbf{F}^-$ 3 trapped electrons	[7, 9–11]
O^--center	Single electron freed from O^{2-} by absorption of a UV photon	[8]

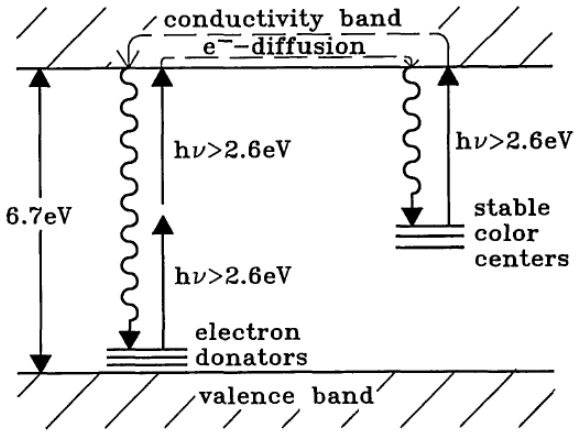

Figure 1.1: Representation of proposed mechanisms for color center generation (from [5]).

A few simple models have been proposed to explain both transient (short-lived) and stable (long-lived) color center creation in YAG [5, 8, 9]. Figure 1.1 [5] demonstrates two of these

proposed mechanisms of color center generation. Single- or multiple-photon excitation of electrons from the valence band to the conduction band can form O^--centers, which are reported to have ground state energies above the valence band [5,9]. These excited electrons could fall immediately back into their original state, reverting O^- back to O^{2-} [9]. This process is a proposed explanation for the creation and elimination of transient color centers.

Electrons excited into the conduction band could also be trapped by a stable defect state, such as an oxygen vacancy, upon relaxation. This process is a proposed mechanism for stable color-center generation and is outlined in Figure 1.1 [5]. While these models are useful for understanding the general processes through which defects are induced, no specific defect energy levels have been determined.

In the years since the discovery of laser action in Nd:YAG, many groups have studied color center defects in YAG. However, most of these studies were limited in the sense that they focused on absorption features observed in samples of rare-earth–doped and undoped YAG. Table 1.2 summarizes the YAG absorption features identified in the literature over the past four decades.

While the majority of the spectroscopic features reported in YAG have been absorption bands, a few YAG defect emission features have also been reported in the literature [7, 12]. Bernhardt observed YAG fluorescence at 525 nm and 570 nm under 470 nm excitation [12]. He also detected emission at 647 nm and 672 nm with 310 nm excitation [12]. Bernhardt determined that these peaks were caused by Mn^{4+}, and Fe^{3+} impurities [12]. Pujats reported two fluorescence peaks at 400 nm under 370 nm excitation and ∼460 nm with 240 nm excitation [7]. Pujats attributed these fluorescence features to F^+-centers and F-centers, respectively [7].

In addition to the many cited absorption features and the few reports of observed defect emission, there are several findings that serve as milestones in the history of YAG color center investigation. For example, in 1967, three years after the discovery of laser oscillations in Nd:YAG, Bass and Paladino discovered stable color centers in undoped YAG [13]. While color centers had been observed before in alkali halides, this was the first report of analogous defects in YAG. In [13], the excitation of these color centers was attributed to exposure of the crystal to intense ultraviolet radiation in the 200–400 nm wavelength range. The

Table 1.2: Defect absorption features reported in the literature

Wavelength (nm)	**Proposed Defect**	**Reference**
195	F center	[7]
226	—	[10]
240	F center	[7]
254	Fe^{2+} impurities	[9]
258	Fe^{2+} impurities	[10]
310	—	[2, 13]
310	Mn^{4+} impurities	[12]
313	Fe^{2+} impurities	[9]
353	F center	[7]
360	F or F^+ center	[10]
403	—	[9]
450	Mn^{4+} impurities	[12]
470–480	Fe^{3+} impurities	[12]
480	F or F^+ center	[10]
495	F center	[7]
526	F or F^+ center	[10, 11]
543	—	[9]
625	—	[2]
830	F or F^+ center	[10]
833	F center	[9]

UV-induced, stable absorption feature did not diminish over time, and Bass and Paladino predicted that annealing at temperatures greater than 100 °C would be necessary to restore the crystal to its original state of clarity [13].

One year later, G. Zeidler found that laser output power doubled in an arc-lamp pumped Nd:YAG laser system when the visible and ultraviolet wavelengths below 500 nm were filtered out of the pump light [3]. He also found that when the Nd:YAG rod was pumped with unfiltered light from the krypton arc lamp, the peak intensity of each laser pulse preceded the peak intensity of the pump light by 30 μs whereas, when the pump light below 500 nm was attenuated, the peak intensities of both the laser pulse and pump coincided. From these findings, Zeidler concluded that there were short-lived color centers present in Nd:YAG that were excited by photons of wavelength less than 500 nm and were detrimental to laser performance [3].

Also in 1968, Willis and Dixon observed a transient color center generated by 300 nm irradiation that exhibited a broad absorption feature peaking at 625 nm and extending as far into the infrared as 1064 nm—the fundamental lasing wavelength of Nd:YAG [2]. This range of absorption also encompasses the most favorable pump wavelengths for Nd:YAG (750–825 nm). At 1064 nm, the absorption coefficient was found to be 2% cm^{-1} [2]. This result was the first explicit citation of 1064 nm absorption by color centers in Nd:YAG. These results were reinforced in 1973 by K. Mori, who found the transient absorption coefficient of Nd:YAG at 1064 nm to be as high as 4% cm^{-1} immediately after unfiltered pumping from a krypton arc lamp [14]. These results plainly indicate that color center defects have profound implications for the performance of Nd:YAG lasers.

In summary, since the first publication of the Nd:YAG laser, tentative links have been made between specific types of defects and absorption and emission bands, and models have been proposed to explain the optical excitation of both transient and stable color centers. However, little effort appears to have been devoted to systematically probing the full energy structure of defects in YAG. Gaining comprehensive knowledge of this energy structure and the flow of energy within the crystal could be the first step toward isolating and minimizing specific detrimental defects in rare-earth–doped YAG.

CHAPTER 2

MEASURING ABSORPTION SPECTRA OF YAG AND Nd:YAG

Five samples of undoped YAG and twelve samples of Nd:YAG were provided for this study by VLOC, Inc. The twelve doped samples varied in Nd concentration from 0.4–1.4 % by atomic weight. Before any invasive probing of YAG defects was performed, CW absorption spectra of the provided samples were measured. Collection of baseline absorption spectra was crucial. These spectra serve as a metric against which to compare future absorption measurements of samples in which stable color centers may have been induced either unintentionally or deliberately. Also, any features detected in these absorption spectra that had not been observed in previously recorded Nd:YAG absorption spectra would have provided early evidence of stable color centers in the samples provided.

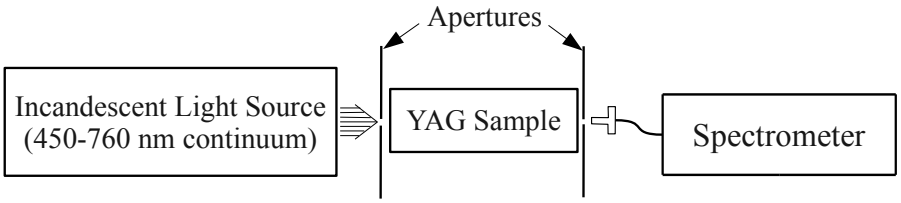

Figure 2.1: Experimental arrangement for CW absorption spectra measurements in the 450–770 nm region.

Three different experimental configurations were used to record sample absorption spectra. The setup represented in Figure 2.1 utilized a filament lamp to create a broad continuum in the 450–770 nm range. This continuum was directed through an aperture (d$\sim$3 mm) and into the sample under investigation. The light was then directed through another aperture and into the spectrometer fiber. Detection of spectra in this configuration was accomplished with an Ocean Optics SD2000 fiber-coupled spectrometer. This is a dual-grating spectrometer with a spectral range of $\sim$250–1100 nm and spectral resolution of $\sim$0.5 nm. Spectra were

collected from each of the samples provided, and a representative spectrum provided by this setup is shown in Figure 2.2. Undoped YAG exhibited no appreciable absorption in this wavelength range and the doped samples exhibited no absorption features unaccounted for in past Nd:YAG absorption measurements [15, 16].

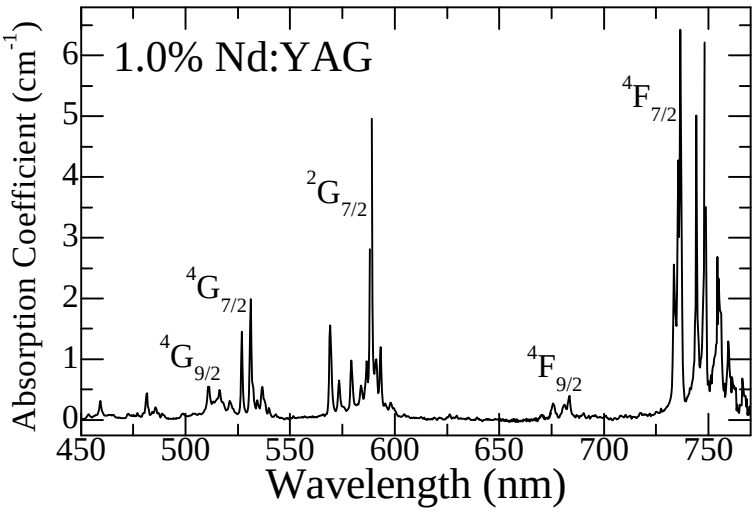

Figure 2.2: Representative absorption spectrum of 1.0% at. wt. Nd:YAG in the 450–770 nm region. The terminal states for several groups of transitions are indicated.

The second experimental arrangement used to measure absorption is represented by Figure 2.3. In this setup, a wavelength-tunable CW Ti:Sapphire laser with a tuning range of 760–860 nm was used as the radiation source. With the laser tuned to a fixed wavelength, both the unobstructed laser power and the power transmitted through the sample of interest were measured with a pyroelectric detector. The laser wavelength was tuned in increments of $\sim$1 nm and power readings were recorded at each wavelength step. With these power measurements, spectra such as that shown in Figure 2.4 were produced. As was the case in the absorption experiments performed with the filament lamp, no features were observed in these spectra that had not been reported previously [15, 16].

Lower resolution, but more spectrally comprehensive, measurements of the sample absorption spectra were made with a Varian Cary spectrophotometer. A representative spectrophotometric trace of one of the samples, recorded from 300–3300 nm, is shown in Figure 2.5. In the Nd:YAG spectra collected with the spectrophotometer, absorption from the ground state

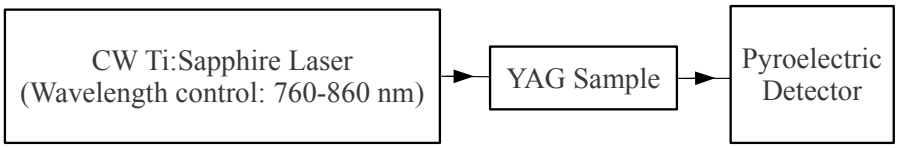

Figure 2.3: Experimental arrangement for CW absorption spectra measurement in the 760–860 nm region.

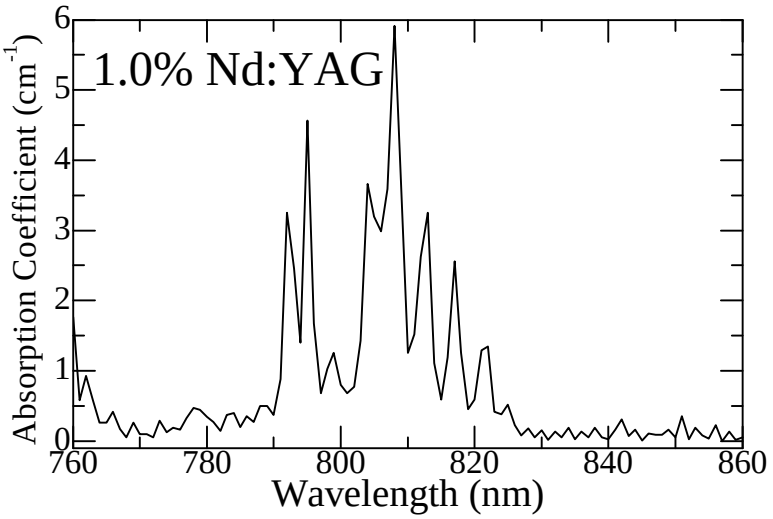

Figure 2.4: Representative absorption spectrum of 1.0% at. wt. Nd:YAG in the 760–860 nm region.

of Nd^{3+} ($^4I_{9/2}$) to the $^4I_{15/2}$ and $^4I_{13/2}$ state manifolds is observed as marked in Figure 2.5.

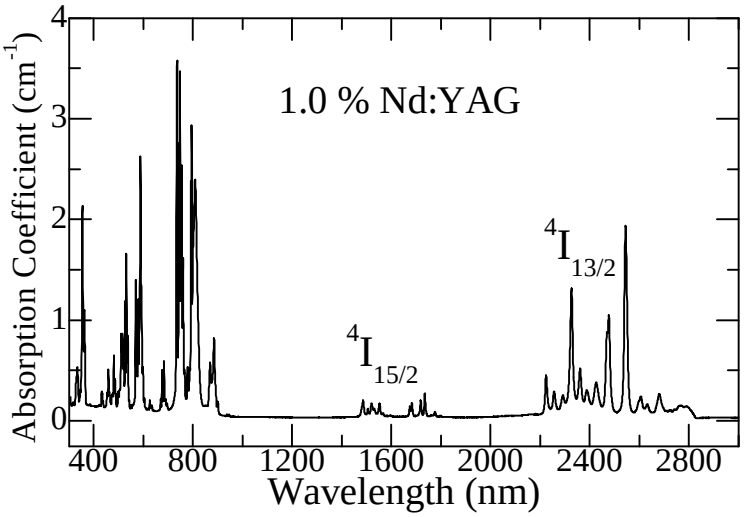

Figure 2.5: Absorption spectrum of 1.0% at. wt. Nd:YAG in the 300–3000 nm region. The terminal states for two groups of transitions are indicated.

It is prudent to note that there are nonnegligible differences in the peak amplitudes of the absorption measured using the first two setups and that measured with the spectrophotometer. These differences are primarily due to the fact that the wavelength resolution of the spectrophotometer is coarser than that of the spectrometer used in the first two setups. This results in undersampling of the sharp absorption features of Nd:YAG in the 450–860 nm range by the spectrophotometer which is manifested in the inaccurate amplitudes of the measured absorption coefficient at those wavelengths.

CHAPTER 3

ULTRAVIOLET-EXCITED DEFECT FLUORESCENCE

In the past, emission spectra of YAG have been studied over small wavelength ranges ($\leq$200 nm) and mainly have been analyzed to determine spectral characteristics of impurities in YAG (such as the presence of Mn^{4+} and Fe^{3+} ions) rather than lattice defects (such as O^{-}-centers and F-centers) [7, 12]. However, defect emission spectra are rich sources of data for determining the energy structure and dynamics of lattice defects. From these spectra, sample impurities can be readily identified. Also, by monitoring the decay of the emission intensity at fixed wavelengths, emission features can be linked to common excited defect states.

3.1 Fluorescence in Undoped YAG

Using ultraviolet laser sources to excite the samples, sample fluorescence was collected by an Ocean Optics SD2000 fiber-coupled spectrometer. According to the literature, the F-center defect in YAG has an absorption peak at 240 nm [7]. Also, Innocenzi et al. found the absorption coefficient of YAG from 200–350 nm to be non-negligible [17]. Because its wavelength is close to 240 nm and is within the aforementioned range of YAG absorption, a KrF excimer laser (λ =248 nm) was chosen as the first excitation source in this series of experiments. Figure 3.1 represents the experimental arrangement used to collect these data.

The emission spectrum recorded from a sample of undoped YAG is shown in Figure 3.2. To the eye, the crystal appears orange, which is consistent with the intense, broad ($\sim$50 nm FWHM) feature centered at 600 nm in the fluorescence spectrum. The bandgap of YAG is 6.73 eV while the energy of a 248 nm photon is 5 eV [18]. Therefore, any fluorescence

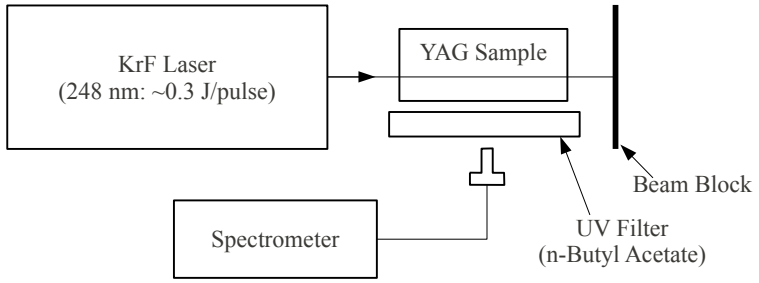

Figure 3.1: Experimental setup diagram for the measurement of fluorescence spectra.

observed from excitation of undoped YAG at 248 nm is surely caused by a lattice defect, an impurity in the sample, or a multiphoton absorption process. The spike in the fluorescence spectrum at 688 nm as well as the two bands on either side of it are attributed to emission from Cr^{3+} impurities. Figure 3.3 illustrates this, comparing the portion of the undoped fluorescence spectrum from 650–730 nm with a previously published Cr:YAG nanocrystal emission spectrum [19]. However, the rest of the features in this emission spectrum have not been reported previously and appear to be due to defects in the YAG sample. This observation provides not only proof of the presence of defects but also a first glance at the energy flow among them.

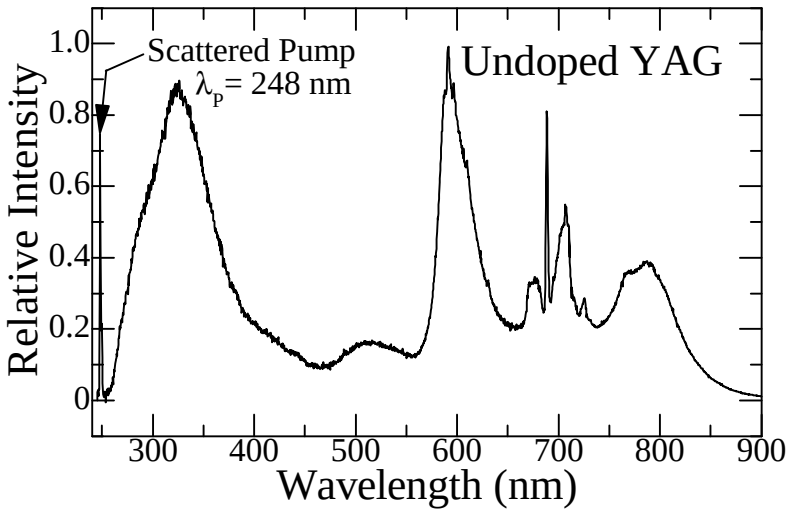

Figure 3.2: Fluorescence spectrum of undoped YAG pumped with a KrF laser (λ =248 nm).

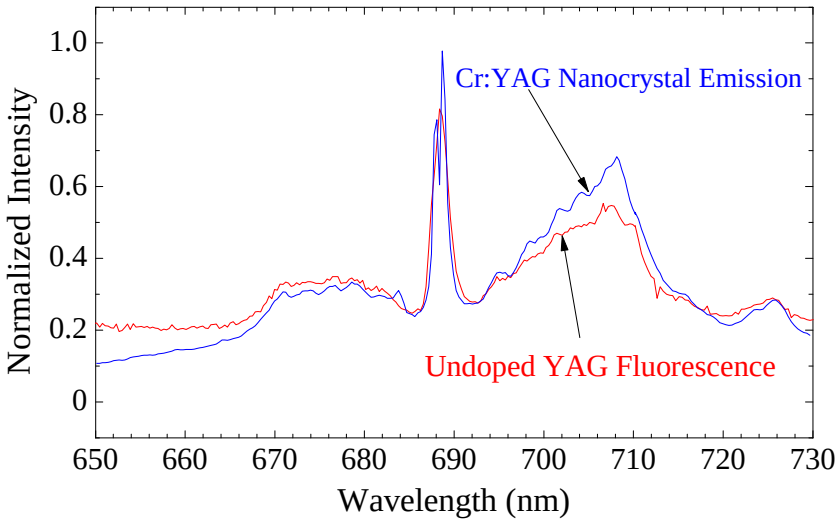

Figure 3.3: Undoped YAG fluorescence superimposed with Cr:YAG nanocrystal fluorescence spectrum from 650–730 nm [19].

3.2 Evidence of Multiphoton Processes and Excitation of Stable Color Centers in YAG

Varying the fluence of the KrF laser reveals non-linear variation of the relative intensities of several features in the fluorescence spectrum of YAG. Specifically, the fluorescence of Cr^{3+} increases disproportionately as the laser fluence increases, as shown in Figure 3.4. This implies the occurrence of multi-photon processes that enhance the coupling of energy into Cr^{3+}.

High KrF fluence has also been demonstrated to excite long-lived color centers in YAG, as shown in Figure 3.5. In this figure, samples 1 and 2 were previously colored by high-energy KrF pulses (>25 mJ) as evidenced by the increase in relative intensity of the Cr^{3+} fluorescence features in their spectra. This implies that there are long-lived color centers within samples 1 and 2 that enhance energy coupling into the Cr^{3+} ion. The differences between the relative fluorescence intensity of Cr^{3+} in samples 1 and 2 may be due to a slow time-decay of these long-lived color centers. Both samples were exposed to 300 mJ KrF pulses, but sample 1 was exposed several days before sample 2. This could explain why the Cr^{3+} fluorescence is relatively less intense in sample 1 than in sample 2. In contrast,

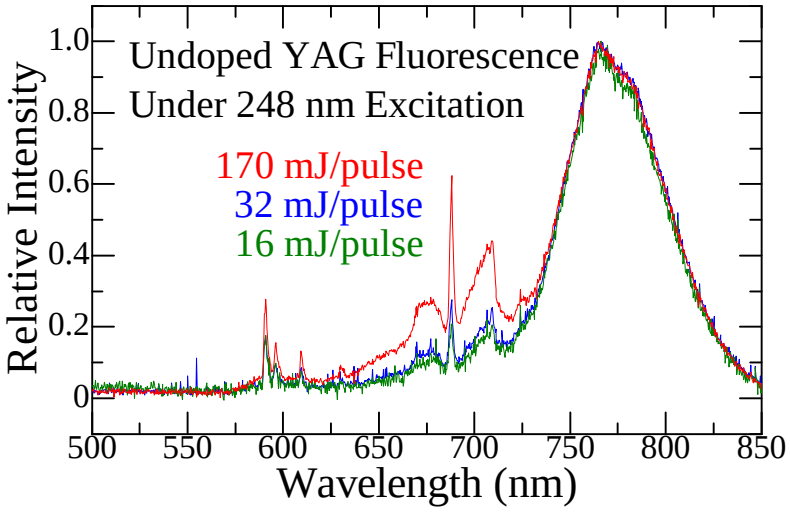

Figure 3.4: YAG fluorescence as incident fluence is varied.

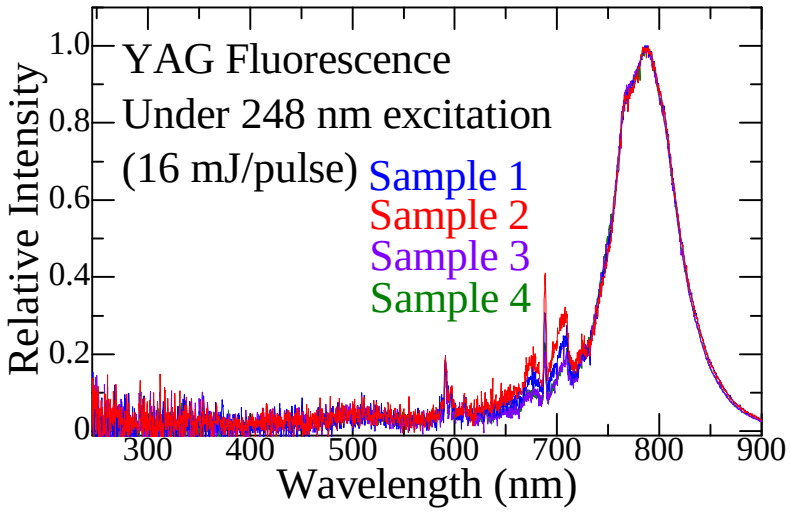

Figure 3.5: Fluorescence spectra of two colored (1 and 2) and two uncolored (3 and 4) YAG samples.

samples 3 and 4 were not exposed to high-energy KrF pulses, and their spectra appear to be relatively identical.

3.3 Comparison of Fluorescence Measurements from Different Samples

Of the five undoped YAG samples provided for this study, four were cleaved from the same boule after growth. Fluorescence measurements indicate that the density of defects varies between different boules even within the same growth facility. This is illustrated in Figure 3.6, which shows drastic differences in the shapes and relative intensities of fluorescence features between the two samples. Recall Figure 3.5 which shows the fluorescence spectra of the

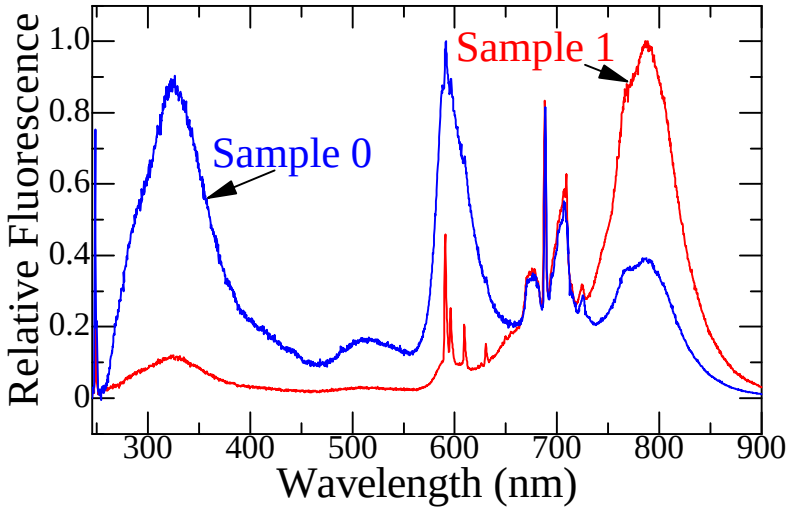

Figure 3.6: Fluorescence from two samples of undoped YAG superimposed.

four undoped samples from a common boule and their spectral similarity. Non-uniformities between boules imply that the formation of color center defects during crystal growth could be highly sensitive to interactions between the molten salts and the crucible. The unique sample was used for many of the experiments discussed in this thesis because it has more pronounced spectral features in the visible spectral range than do the other undoped samples.

3.4 Fluorescence in Nd:YAG

Photoluminescence spectra from Nd:YAG samples were also recorded, and several fluorescence features were found to be common to both the undoped and Nd-doped spectra. Figure 3.7 shows the undoped YAG spectrum in purple overlaid with the Nd:YAG spectrum in green. The two spectra are normalized to the shared fluorescence features in the 750–825 nm region. In this region of the spectrum, the Nd^{3+} ions have absorbed some of the fluorescence

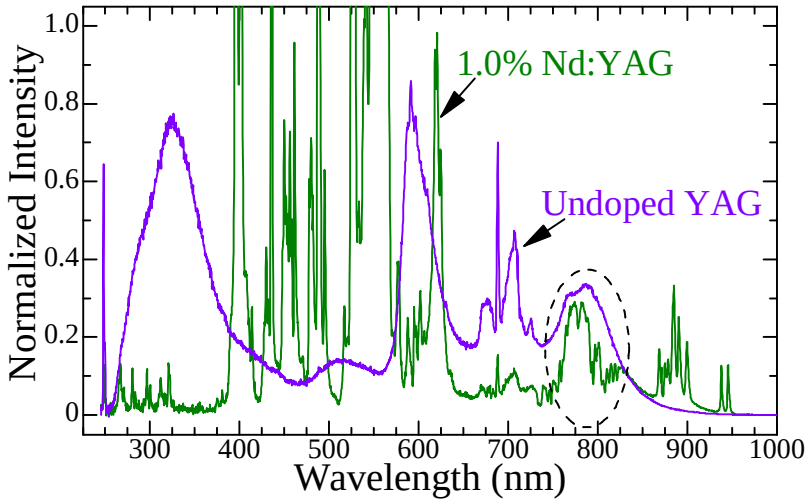

Figure 3.7: Fluorescence spectra of undoped YAG and Nd:YAG normalized to the circled spectral feature from 750–825 nm (λ_P =248 nm).

originating from color center defects in the YAG host. This is explicitly illustrated in Figure 3.8, which shows the subtraction of the Nd:YAG fluorescence from that of undoped YAG overlaid with the NIR absorption spectrum of Nd:YAG measured in the aforementioned absorption experiments. In this figure, the overlap of Nd:YAG absorption features with the features in the subtracted spectra is undeniable, and this overlap provides explicit evidence of optical coupling of YAG defects and Nd^{3+} ions in this wavelength range. Stated another way, the data of Figures 3.7 and 3.8 show clearly that the Nd^{3+} ion absorbs near-IR emission emanating from a defect in the crystalline lattice. This indicates that the primary energy transfer mechanism between defects and Nd^{3+} ions in this region is via photon transfer.

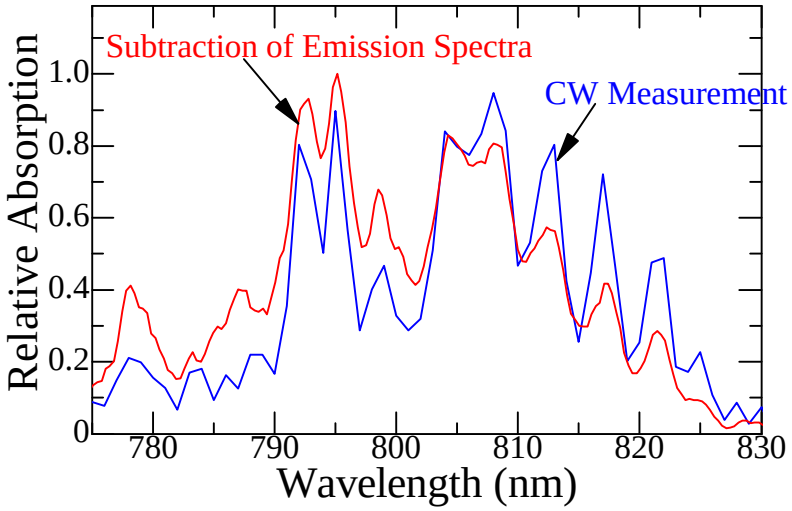

Figure 3.8: Difference of undoped YAG and Nd:YAG fluorescence spectra superimposed onto the CW measurement of Nd:YAG absorption in the 775–830 nm region.

3.5 Comparison of Fluorescence from 248 nm and 355 nm Excitation

After successfully generating photoluminescence with KrF excitation at 248 nm, more YAG emission spectra were measured using the third harmonic of an Nd:YAG laser (355 nm) as the excitation source. This wavelength is close to the cited absorption wavelength of 360 nm of the F^--center in YAG [7]. A 355 nm photon has an energy of 3.5 eV, so any fluorescence features observed in the KrF-induced emission spectrum of YAG that are not present in the Nd:YAG third-harmonic–induced spectrum are likely due to excited states with energies greater than 3.5 eV above the valence band of YAG. The fluorescence spectrum of undoped YAG under Nd:YAG third-harmonic excitation is shown in green in Figure 3.9. Compared with the 248 nm-induced spectrum, this spectrum appears to be much less congested, having only one broad, visible feature with a maximum intensity at 525 nm. This lack of complex fluorescence structure suggests that most of the fluorescence features in the 248 nm-induced spectrum radiate from excited states lying $\geq$3.5 eV above the valence band of YAG. However, as shown in Figure 3.9, the two spectra appear to have the 525 nm fluorescence feature in common, as the longer-wavelength-side slope of this feature is consistent with the slope of the 248 nm fluorescence spectrum in that region.

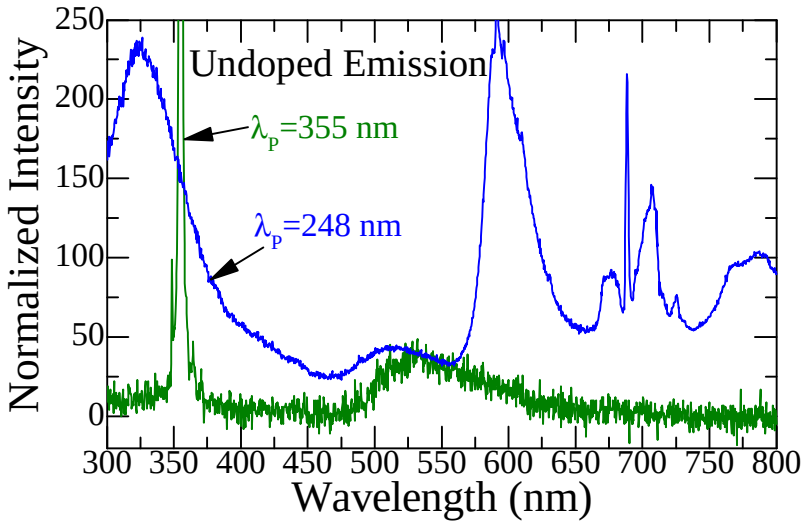

Figure 3.9: 248 nm- and 355 nm-induced fluorescence spectra superimposed and normalized to the fluorescence feature centered at 525 nm.

CHAPTER 4

DEFECT FLUORESCENCE DECAY

In order to clarify the relationships between the features in the emission spectrum of Figure 3.2, measurements were made of the time-resolved intensity of several of these features. Finding common decay parameters between emission features at different wavelengths has linked several of these features to a common excited state and, therefore, to a common defect. Making these links is crucial for determining the energy structure of each specific defect in the medium.

4.1 Fluorescence Decay Measurements

To make these measurements, optical bandpass filters were used to isolate features of the 248 nm-induced fluorescence while a photomultiplier (PMT) was used to measure the decay of the fixed-wavelength fluorescence. The experimental setup used is represented in Figure 4.1. As shown in this figure, an n-butyl acetate filter was used in addition to the bandpass filter to prevent any scattered 248 nm pump light from reaching the photomultiplier tube. Five different features of the fluorescence spectrum were isolated in this experiment, and the transmission curves of the bandpass filters used are plotted atop the 248 nm-induced undoped YAG fluorescence spectrum in Figure 4.2.

The resulting measurements from this experimental arrangement were fit with double exponential curves. Figure 4.3 is a plot of the measured decay at 800 nm, fit with a double exponential curve with the parameters shown. Similar fits were found for each of the other isolated features shown in Figure 4.2, and the extracted decay constants from all these fits are compiled in Table 4.1.

As is shown in Figure 4.2, the bandpass filters used for wavelength isolation were not

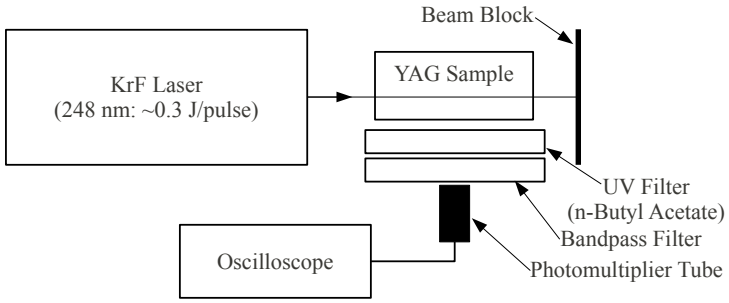

Figure 4.1: Experimental setup diagram for decay constant measurement.

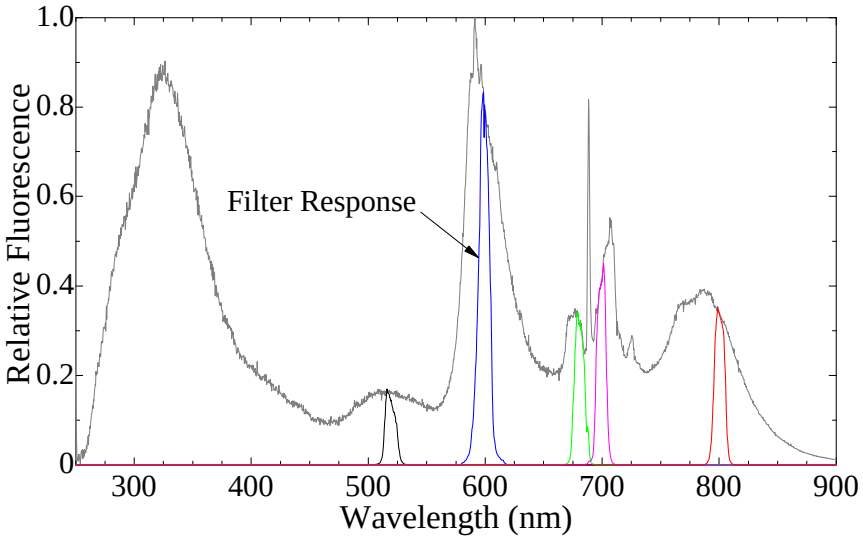

Figure 4.2: Bandpass filter response curves superimposed onto 248 nm-induced fluorescence spectrum of undoped YAG.

sharply resolved because the spectral width (FWHM) of the filters is nominally 10 nm. Also, as shown in Figure 4.3, as the fluorescence intensity decreases, PMT noise becomes nonnegligible and factors into the curve fitting. Experimental uncertainties of the decay constants are estimated to be ±10%, which is dominated by the broad acceptance bandwidth of the bandpass filters and, for long decay times, PMT noise.

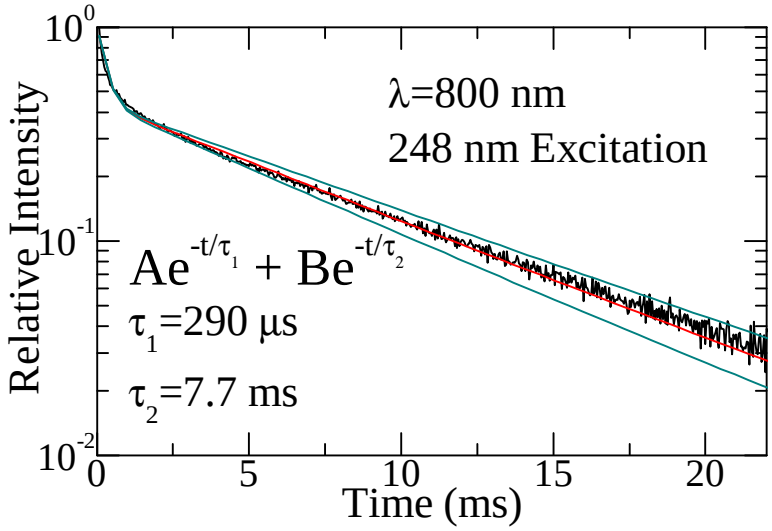

Figure 4.3: Representative fluorescence decay fit with a double exponential curve, shown in red. $\tau_2 \pm 10\%$ curves shown in cyan.

Table 4.1: Decay constants extracted from exponential fits of fluorescence decay

Wavelength (nm)	τ_1 (μs)	τ_2 (ms)
520	160	1.6
591	190	1.8
678	70	1.1
708	50	0.9
800	290	7.7

With this uncertainty in mind, the exponential fit curves for the decay of the fluorescence at both 520 nm and 591 nm produced decay constants that are, to within experimental uncertainty, identical. Thus, both can be attributed to the same excited defect state. The extracted decay constants for the features at 678 nm and 708 nm are also equal to within experimental error, implying that these features can be similarly linked. This linkage between

the 678 nm and 708 nm features was expected, because as was shown in Figure 3.3, these features have been attributed to Cr^{3+} impurities.

4.2 YAG Fluorescence at Liquid Nitrogen Temperature

In the fluorescence spectrum of YAG, there are several broad fluorescence features that appear to be the sum of several smaller features, but because of phonon broadening of the fluorescence, these individual contributors cannot be resolved. However, determining the underlying peaks of these broad features will greatly facilitate future decay measurements, revealing key wavelengths to isolate. Therefore, in an attempt to narrow the spectral widths of the discrete features in the YAG fluorescence, a cryostat was used to cool the YAG sample to liquid nitrogen temperature (LNT=77 K). A new fluorescence spectrum of the sample was taken at 77 K and is shown in Figure 4.4, overlaid with the spectrum measured at room temperature (∼300 K). It is evident from this figure that the broad spectral feature centered

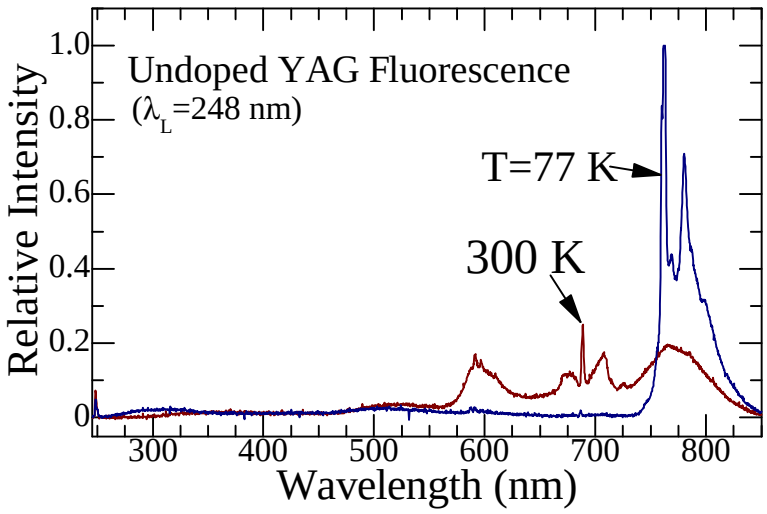

Figure 4.4: Overlaid fluorescence spectra of undoped YAG at 300 K and 77 K.

at 600 nm as well as the Cr^{3+} features which fluoresce intensely at room temperature suffer a drastic decrease in their fluorescence strength when the sample is cooled to 77 K. This implies that the energy states from which these features originate are accessed primarily via phonon-assisted energy transfer. Conversely, the fluorescence feature centered at 775 nm at

room temperature increases dramatically in intensity and resolves into two large peaks and several smaller peaks when the crystal is cooled to 77 K.

In addition to measuring the crystal fluorescence at 77 K, fluorescence was monitored while the sample cooled. Figure 4.5 shows this progression. As the temperature decreases, the

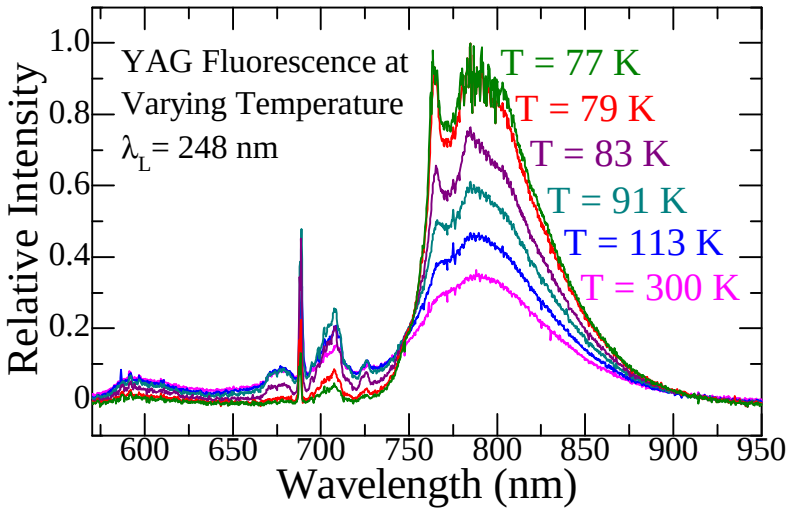

Figure 4.5: Evolution of fluorescence of undoped YAG as the temperature drops.

fluorescence feature centered at 800 nm gradually increases in overall intensity. It also begins to split into two distinct peaks as the temperature drops below 100 K. As the temperature nears 77 K in this series of plots, the detector begins to saturate, which explains the noise in the spectrum at 800 nm.

Most of the other features in this spectrum fade away as the crystal cools, but the Cr^{3+} fluorescence actually increases in intensity initially before decreasing. This phenomenon is shown in Figure 4.6.

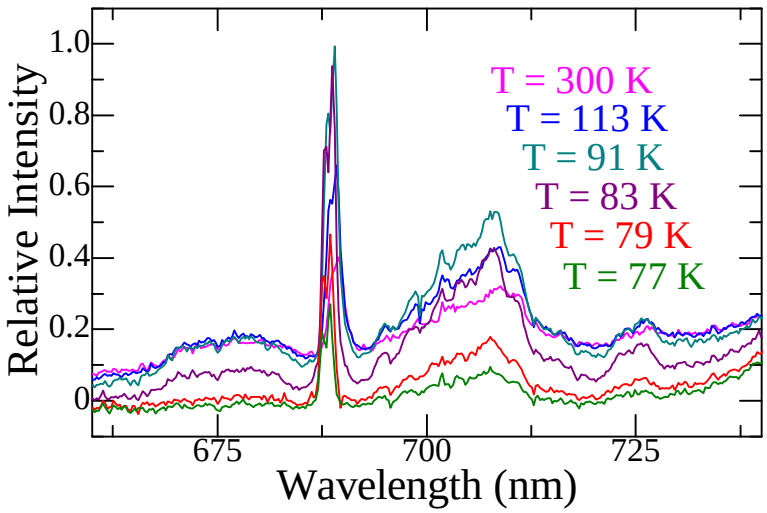

Figure 4.6: Evolution of fluorescence of undoped YAG as the temperature drops.

CHAPTER 5

CONCLUSIONS

In this thesis, several techniques were employed to investigate the energy structure and flow of energy among defects in YAG. Broadband absorption measurements were made of YAG and Nd:YAG samples, but no defect absorption features were detected in these spectra. This implies that, although color center defects are known to hinder laser action in YAG-based systems, the density of such defects in these media is below the detection limit for the absorption measurement techniques employed in this study.

Emission spectra were also recorded under 248 nm and 355 nm excitation. These spectra provide evidence of the presence of defects in the samples provided by VLOC as well as evidence of the interaction between defects and Nd^{3+} dopants within the medium. Also found in the fluorescence spectra were features indicative of the presence of Cr^{3+} in the doped and undoped YAG samples. The differences between the 248 nm- and 355 nm-induced fluorescence spectra in undoped YAG indicate that many of the fluorescence features in the 248 nm-induced spectra radiate from states that lie between 3.5 eV and 5 eV from ground.

Fluorescent decay of many of the features of the 248 nm-induced YAG emission spectrum was measured and several discrete energy states were identified based on extracted decay parameters. Cooling of the crystals to 77 K revealed the underlying structure of several broad fluorescence features observed in undoped YAG at room temperature. This information can be used to make more systematic decay measurements in the future, because the discrete wavelengths of the narrowed fluorescence features can easily be extracted from the cooled crystal spectra. It would be instructive to observe the decay of the fluorescence at these discrete wavelengths. Also, the evolution of the fluorescence as the sample is cooled from 300 K to 77 K demonstrates the effects of decreased phonon transfer between defects and impurities on the relative intensities of fluorescence features.

The most fruitful experiments outlined in this thesis were based on measuring UV-excited defect fluorescence features. These experiments could be performed using other ultraviolet pump laser sources, such as a frequency-quadrupled Nd:YAG laser (λ=266 nm) or an optical parametric amplifier (OPA). Varying the excitation source could reveal different fluorescence behavior than what has been observed in this thesis. Using an OPA could be particularly interesting because it would allow for tunability of the excitation wavelength, which could be used to further resolve the relative energy differences between excited defect states.

As more fluorescence features are linked to defect excited states, the explicit emergence of the energy structure of the defects as well as the flow of energy among the defects in YAG will follow. With the defect energy structure and flow determined, absorption and emission characteristics can be assigned to individual defects with confidence. With this information, crystal growers will be able to isolate detrimental defects and more accurately determine growth parameters necessary to minimize their presence in future batches of rare-earth–doped YAG.

REFERENCES

[1] J. E. Geusic, H. M. Marcos, and L. G. van Uitert, "Laser oscillations in Nd-doped yttrium aluminum, yttrium gallium and gadolinium garnets," *Appl. Phys. Lett.*, vol. 4, no. 10, pp. 182–184, 1964.

[2] J. B. Willis and M. Dixon, "Assessment and control of imperfections in crystals for laser devices," *J. Cryst. Growth*, vol. 3, pp. 236–240, 1968.

[3] G. Zeidler, "Pump-power-dependent efficiency in a YAG:Nd^{3+} laser," *IEEE J. Quant. Electron.*, vol. 4, pp. 1016–1017, 1968.

[4] B. Henderson and R. H. Bartram, *Crystal-Field Engineering of Solid-State Laser Materials*. Cambridge, UK: Cambridge University Press, 2000.

[5] G. Phillipps and J. Vater, "1.06-μm absorption caused by stable color centers in flash-lamp-pumped Nd:YAG laser rods," *Appl. Opt.*, vol. 32, pp. 3210–3216, 1993.

[6] M. K. Ashurov, Y. K. Voronko, V. V. Osiko, A. A. Sobol, and M. I. Timoshechkin, "Spectroscopic study of stoichiometry deviation in crystals with garnet structure," *Phys. Stat. Sol. (a)*, vol. 42, pp. 101–110, 1977.

[7] A. Pujats and M. Springis, "The F-type centers in YAG crystals," *Radiat. Eff. Defects Solids*, vol. 155, pp. 65–69, 2001.

[8] J. Kvapil, J. Kvapil, and B. Perner, "O^- centre formation in yag crystals doped with rare earth ions," *Krist. Tech.*, vol. 10, pp. 161–165, 1975.

[9] K. Mori, "Transient color centers caused by uv light irradiation in yttrium aluminum garnet crystals," *Phys. Stat. Sol. (a)*, vol. 42, pp. 375–384, 1977.

[10] J. Kvapil, J. Kvapil, J. Kubelka, and V. Kubeček, "Transient absorption and laser output of YAG:Nd," *Czech. J. Phys. B*, vol. 31, pp. 644–651, 1981.

[11] K. Čermák, "Optical polaron absorption in YAG:Nd," *Czech. J. Phys. B*, vol. 31, pp. 1172–1176, 1981.

[12] Hj. Bernhardt, "Formation of biparticles in nominally undoped $Y_3Al_5O_{12}$ crystals?" *Phys. Stat. Sol. (a)*, vol. 31, pp. 365–370, 1975.

[13] M. Bass and A. E. Paladino, "Color centers in yttrium gallium garnet and yttrium aluminum garnet," *J. Appl. Phys.*, vol. 38, pp. 2706–2707, 1967.

[14] K. Mori, "Detection of transient absorption in yag laser crystals using combined laser," *Japan. J. Appl. Phys.*, vol. 12, pp. 325–326, 1973.

[15] Z. Mierczyk, S. Kaczmarek, and K. Kopczyński, "Analysis of absorption spectra of the crystals for coherent radiation pumped solid-state lasers," in *Proc. SPIE*, 1996, pp. 139–142.

[16] T. Y. Fan and R. L. Byer, "Diode laser-pumped solid-state lasers," *IEEE J. Quantum Electron.*, vol. 24, pp. 895–912, 1988.

[17] M. E. Innocenzi, R. T. Swimm, M. Bass, R. H. French, and M. R. Kokta, "Optical absorption in undoped yttrium aluminum garnet," *J. Appl. Phys.*, vol. 68, pp. 1200–1204, 1990.

[18] G. A. Slack, D. W. Oliver, R. M. Chrenko, and S. Roberts, "Optical absorption of $Y_3Al_5O_{12}$ from 10- to 55000-cm^{-1} wave numbers," *Phys. Rev.*, vol. 177, pp. 1308–1314, 1969.

[19] P. Głuchowski, R. Pązik, D. Hreniak, and W. Stręk, "Luminescence properties of Cr^{3+}:$Y_3Al_5O_{12}$," *J. Lumin.*, vol. 129, pp. 548–553, 2009.